Silicon waveguide integrated $MoTe_2$-Ti Schottky Photodetectors at 1600 nm with high linearity

Hengtai Xiang[1], Jingshu Guo[1,2], Laiwen Yu[1],Liu Liu[1,2], Daoxin Dai[*,1,2,3]
[1] *College of Optical Science and Engineering, State Key Laboratory for Modern Optical Instrumentation, International Research Center for Advanced Photonics, Zhejiang University, Zijingang Campus, Hangzhou, 310058, China.*
[2]*Jiaxing Key Laboratory of Photonic Sensing & Intelligent Imaging, Intelligent Optics & Photonics Research Center, Jiaxing Research Institute Zhejiang University, Jiaxing 314000, China.*
[3]*Ningbo Research Institute, Zhejiang University, Ningbo 315100, China.*
[*]Corresponding Author: E-mail: dxdai@zju.edu.cn

***Abstract*—We propose and demonstrate a silicon waveguide integrated $MoTe_2$-Ti Schottky photodetector. The device has shown a responsivity of 23mA/W when operates at 1600 nm, and has a large linear dynamic range of 0.4mW-1.6mW.**

Keywords—silicon photonics; TMDCs; Schottky Photodetectors; $MoTe_2$;

I. INTRODUCTION

In recent years, silicon photonics[1] has become increasingly popular with the development of some important devices such as spectrometers[2], modulators[3], and photodetectors(PDs)[4]. Among these, photodetectors are crucial for applications such as optical communication, imaging, and sensing. Currently, it is desirable to extend the wavelength band of silicon photonics beyond 1550 nm. However, the large bandgap of silicon, has limited its detection wavelength band.

To overcome this, two-dimensional (2D) materials such as graphene, black phosphorus (BP), and transition metal dichalcogenides (TMDCs) have become a promising solution due to their various bandgap and avoiding material and structure mismatch in the design and fabrication. The graphene bolometers and photoconductors have shown high responsivity and large bandwidth up to 100 GHz[5], however, the dark currents are usually too large. The p-n homojunction PTE graphene can work under zero bias with large bandwidths[6], however, the thermal noise is usually significant. The BP PDs usually have limited bandwidth and bad air stability.

TMDCs such as MoS_2, $MoTe_2$, WS_2, WSe_2 have the advantages of various bandgap, high current on/off ratio, and good stability when compared to zero-bandgap graphene and environmentally sensitive black phosphorus. A waveguide-integrated $MoTe_2$-graphene heterostructure photodetector demonstrated recently exhibits a bandwidth of 24 GHz as well as an external responsivity of 0.2 A/W, which has one of the best performances overall[7]. Normally, these TMDC materials can't direct absorb photon beyond 1550 nm due to their large bandgap of ~1 eV[8]. In recent years, the photodetection wavelength range of TMDC has been extended to 1550 nm by using strain engineering.

Schottky photodetector based on internal photoemission provides one solutions for sub-bandgap photodetection. [9]. Inspired by traditional Si-metal Schottky photodetector[10], we propose a metal-TMDC Schottky junction detector to extend TMDC photodetection wavelength to 1550 nm band and beyond. Fig. 1(a) shows the schematic configuration of the present photodetector. The Si waveguide is covered by Al_2O_3 layer. The active region is the TMDC flake atop the metal-insulator(air)-metal (MIM) plasmonic waveguide. The mode converters are used for the coupling between the Si nanowire waveguide and the MIM waveguide. Here, we selected Titanium and $MoTe_2$ to form a low Schottky junction, which extended the detection wavelength range to 1600 nm (and beyond) through a low barrier about 0.52 eV.

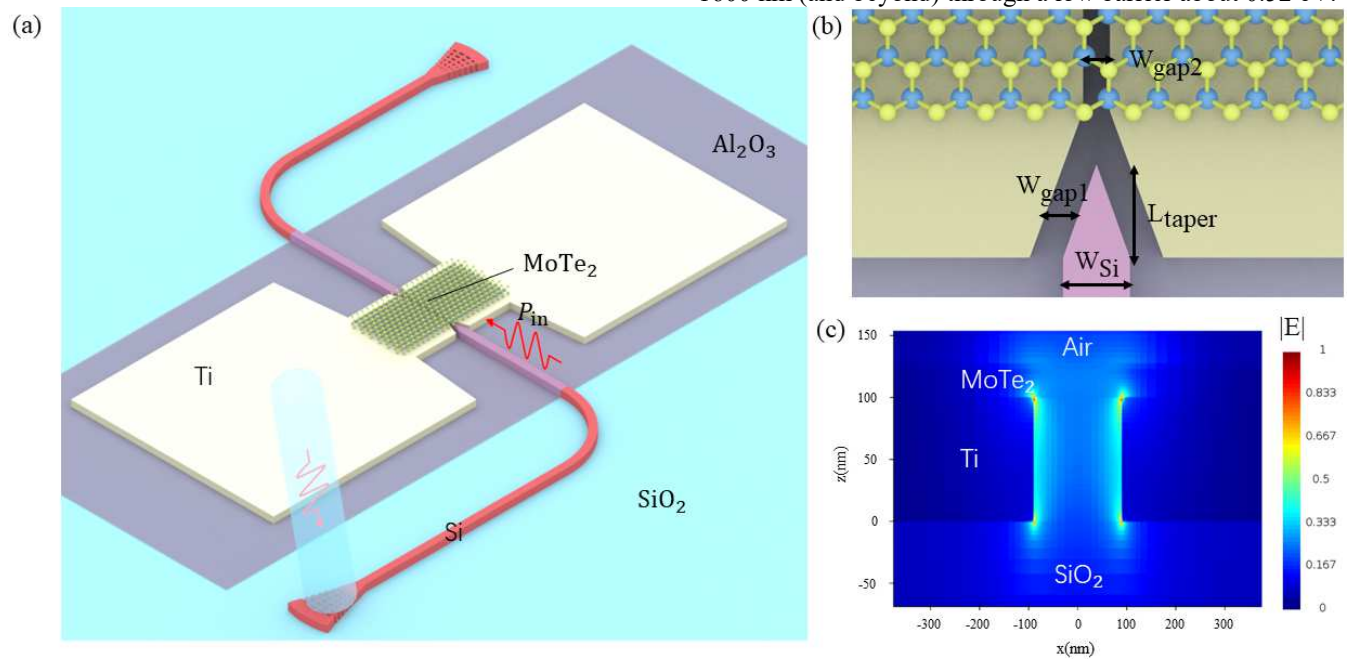

Fig. 1. (a) Schematic configuration of the present $MoTe_2$-Ti Schottky photodetector; P_{in} is the power coupled input the PD (b) Configuration of the mode converter; (c) Simulated electric field profile in the active region at the wavelength of 1600 nm.

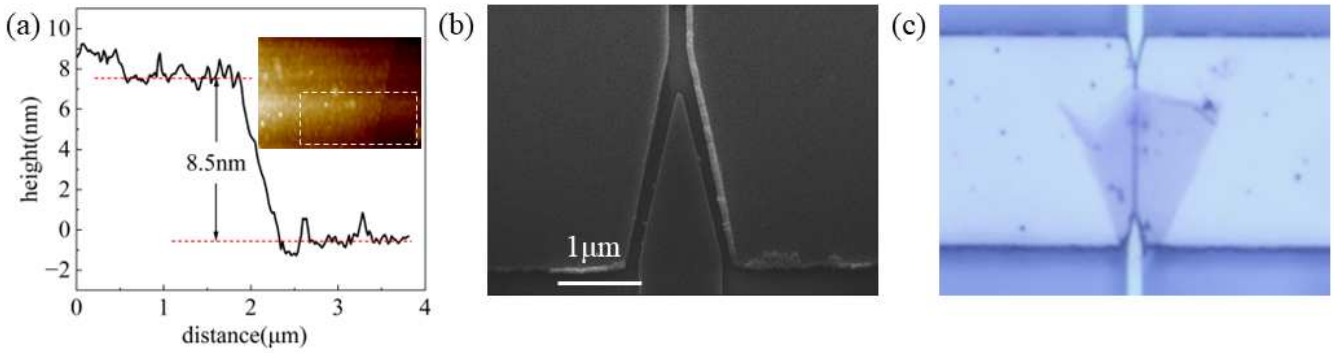

Fig. 2. (a) AFM image of the $MoTe_2$ flake in the active region. The topographic profile along the dashed line shows that the thickness of the $MoTe_2$ flake is about 8.5 nm; (b) SEM picture of the mode converter;(c) Optical microscopy image of the photodetector.

II. DESIGN, FABRICATION AND *MEASUREMENT*

A. Design

The present $MoTe_2$-Ti photodetector operates on the principle that the MIM plasmonic waveguide (i.e., Ti) absorbs the incident light and then photocurrent generates in the two back-to-back $MoTe_2$-Ti Schottky diodes by internal photoemission. Fig. 1 (b) shows the configuration of the mode converter between the Si nanowire waveguide and the MIM waveguide. We performed the 3D FDTD simulation to investigate the optical absorption feature of the MIM waveguide. The calculated mode field in the active region is depicted in Fig. 1 (c), it can be seen that light is gathered on both sides of the electrode. In our simulation, The Si taper length L_{taper} is 2 μm, the gap between Ti electrode and Si taper W_{gap1} is 150 nm, the gap between Ti electrodes W_{gap2} is 180 nm, the width of Si waveguide W_{si} is 1 μm and the thickness of Ti electrodes is 100 nm. The optical absorbance in the active region is 90% when the length of MIM waveguide is 10μm.

B. Fabrication and Characterization

The presented device has advantage in fabrication ease. The ultrathin silicon core layer (100 nm) was formed from a standard 220 nm-thick SOI wafer by the processes of thermal oxidation and wet etched by buffered oxide etch (BOE) corrosion techniques, the thickness of the silicon core was determined by ellipsometer. E-beam lithography (EBL) and the ICP etching process were used for the fabrication of the passive silicon photonic devices with an etching depth of 100 nm. Subsequently, an insulator layer (10-nm-thick Al_2O_3 thin film), was deposited on the chip using atomic-layer deposition (ALD) process. Then, the MIM waveguide (100-nm-thick Ti) were fabricated by electron-beam evaporation and lift-off process. Finally, the $MoTe_2$ thin film was transferred onto the active region, covering the MIM waveguide by using the mechanical exfoliation process[11].

We determine the thickness of the transferred $MoTe_2$ flake by atomic force microscopy(AFM)， the thickness is approximately 8.5 nm according to the topographic cross-sectional profile from the AFM image shown in Fig.2(a). Fig.2(b) displays the scanning electron microscopy (SEM) pictures for the fabricated mode converter and a section of MIM waveguide. It can be seen that the device is virtually identical to the simulation model, and the manufacturing error is within exceed 10 nm. Fig. 2(c) shows optical microscopy image of the active region, consisting of a mode converter, MIM waveguide, and $MoTe_2$ flake covering on top of the waveguide. The length of the $MoTe_2$ flake along the direction of light propagation is approximately 8 μm. Due to its excellent mechanical properties, the $MoTe_2$ flake is well suspended on the MIM waveguide.

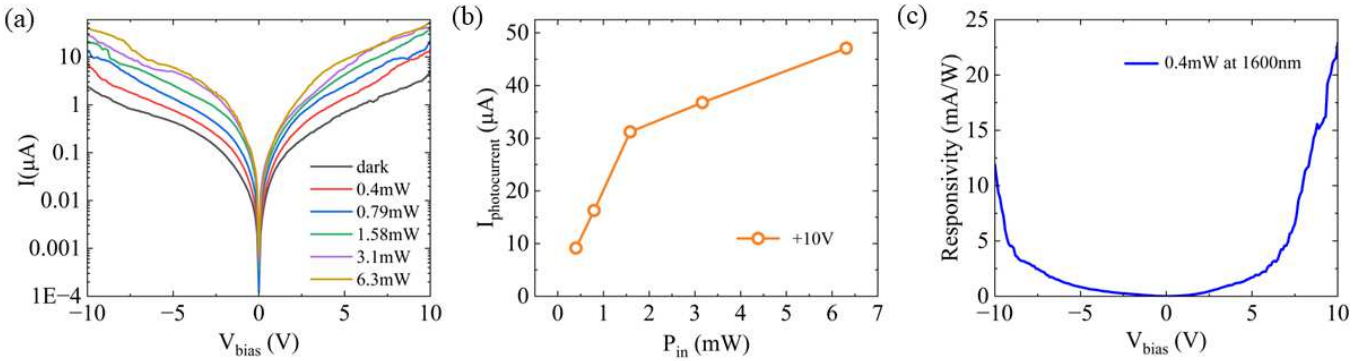

Fig. 3.(a) The measured I-V curves at 1600 nm on a logarithmic scale;(b) Photocurrent as a function of the power coupled into the active area at 10 V; (c)Responsivity as a function of bias voltage at 1600 nm.

C. Measurement

Fig. 3(a) shows the current-voltage (I-V) curves of the present photodetector at wavelength of 1600 nm. Here the power coupled into the active area varies from 0.4 mW to 6.3 mW. The responsivity can reach 23 mA/W when optical power is 0.4mW and 7mA/W when optical power is 6.3mW. The dependence of the photocurrent on the optical power is summarized in Fig. 3(b). Here the bias voltage is fixed at 10V. It can be seen that the photocurrent varies linearly as the input optical power (P_{in}) varies from 0.4 mW to 1.6 mW. Meanwhile the responsivity remains relatively constant in this range, about 20 mA/W and then shows a downward trend when the incident optical power keeps increasing. Due to a large number of negative electrons accumulate in $MoTe_2$ flake, while positive charges accumulate in the Ti electrode when the incident optical power is high, which creates an internal electrostatic field and then blocks the hot electrons. Fig.3(c) shows the relationship between responsivity and the bias voltage. The responsivity-bias voltage curve is almost symmetrical under positive and negative bias voltage because the present photodetector uses a symmetrical back-to-back configuration. The slight differences may be due to incomplete symmetry of the transferred $MoTe_2$ flake. The normalized photocurrent-to-dark-current ratio (NPDR) of the present photodetector is about $1.6 \times 10^4 W^{-1}$.

III. CONCLUSION

In conclusion, through the combination of Ti and $MoTe_2$, we extend the detection wavelength band of TMDC materials. It has realized relatively comprehensive performance, such as responsivity, linear dynamic range, and signal-to-noise ratio. By selecting a better combination of metal and TMDC, it is possible to achieve higher responsivity and wider photodetection wavelength band in the future.

ACKNOWLEDGMENT

This work was supported by National Major Research and Development Program (No. 2018YFB2200200/2018YFB2200203); National Science Fund for Distinguished Young Scholars (61725503); National Natural Science Foundation of China (NSFC) (61905210, 61961146003, 91950205); Zhejiang Provincial Natural Science Foundation (LR22F050001, LD22F040004); Leading Innovative and Entrepreneur Team Introduction Program of Zhejiang (2021R01001); The Fundamental Research Funds for the Central Universities.

REFERENCES

[1] D. Thomson *et al.*, 'Roadmap on silicon photonics', *J. Opt.*, vol. 18, no. 7, p. 073003, 2016.

[2] T. Hu *et al.*, 'Silicon photonic platforms for mid-infrared applications [Invited]', *Photonics Res.*, vol. 5, no. 5, p. 417, 2017.

[3] N. Youngblood, Y. Anugrah, R. Ma, S. J. Koester, and M. Li, 'Multifunctional Graphene Optical Modulator and Photodetector Integrated on Silicon Waveguides', *Nano Lett.*, vol. 14, no. 5, pp. 2741–2746, 2014.

[4] C. Liu *et al.*, 'Silicon/2D-material photodetectors: from near-infrared to mid-infrared', *Light Sci. Appl.*, vol. 10, no. 1, p. 123, 2021,.

[5] P. Ma *et al.*, 'Plasmonically Enhanced Graphene Photodetector Featuring 100 Gbit/s Data Reception, High Responsivity, and Compact Size', *ACS Photonics*, vol. 6, no. 1, pp. 154–161, 2019.

[6] S. Schuler *et al.*, 'High-responsivity graphene photodetectors integrated on silicon microring resonators', *Nat. Commun.*, vol. 12, no. 1, p. 3733, 2021.

[7] N. Flöry *et al.*, 'Waveguide-integrated van der Waals heterostructure photodetector at telecom wavelengths with high speed and high responsivity', *Nat. Nanotechnol.*, vol. 15, no. 2, pp. 118–124, 2020.

[8] X. Liu, M. S. Choi, E. Hwang, W. J. Yoo, and J. Sun, 'Fermi Level Pinning Dependent 2D Semiconductor Devices: Challenges and Prospects', *Adv. Mater.*, vol. 34, no. 15, p. 2108425, 2022.

[9] M. Casalino, G. Coppola, R. M. De La Rue, and D. F. Logan, 'State-of-the-art all-silicon sub-bandgap photodetectors at telecom and datacom wavelengths: State-of-the-art all-silicon sub-bandgap photodetectors at telecom and datacom wavelengths', *Laser Photonics Rev.*, vol. 10, no. 6, pp. 895–921,2016.

[10] J. Guo, Z. Wu, and Y. Zhao, 'Enhanced light absorption in waveguide Schottky photodetector integrated with ultrathin metal/silicide stripe', *Opt. Express*, vol. 25, no. 9, p. 10057, 2017.

[11] A. Castellanos-Gomez *et al.*, 'Van der Waals heterostructures', *Nat. Rev. Methods Primer*, vol. 2, no. 1, p. 58, 2022.